

Quantum Hypothesis Testing for Exoplanet Detection

Zixin Huang^{1,2} and Cosmo Lupo²¹*Department of Physics and Astronomy, Macquarie University, NSW 2109, Sydney, Australia*²*Department of Physics & Astronomy, University of Sheffield, S3 7RH, Sheffield, United Kingdom* (Received 3 June 2021; accepted 2 August 2021; published 23 September 2021)

Detecting the faint emission of a secondary source in the proximity of the much brighter one has been the most severe obstacle for using direct imaging in searching for exoplanets. Using quantum state discrimination and quantum imaging techniques, we show that one can significantly reduce the probability of error for detecting the presence of a weak secondary source, especially when the two sources have small angular separations. If the weak source has intensity $\epsilon \ll 1$ relative to the bright source, we find that the error exponent can be improved by a factor of $1/\epsilon$. We also find linear-optical measurements that are optimal in this regime. Our result serves as a complementary method in the toolbox of optical imaging, with applications ranging from astronomy to microscopy.

DOI: 10.1103/PhysRevLett.127.130502

Hypothesis testing is a fundamental task in statistical inference and has been a crucial element in the development of information sciences. The simplest setting involves a binary decision in which the goal is to distinguish between two mutually exclusive hypotheses, H_0 (the null) and H_1 . For example, an astronomer in search of exoplanets collects data from a portion of the sky and has to decide whether there is (H_1) or there is not (H_0) a planet orbiting around a star. With limited data, this decision is subject to errors. As exoplanets are rare, the experimenters' goal is to minimize the probability of a false negative (type II error). Yet, they may be willing to accept false positives (type I error) as long as they come with a probability below a certain threshold.

In quantum information theory, the two hypotheses are represented by a pair of quantum states ρ_0, ρ_1 . Given n copies of the state, we denote as α_n the probability of a type I error, and β_n is the probability of a type II error. According to the quantum Stein lemma [1,2], if we require $\alpha_n \in (0, \delta)$, with $\delta < 1$, then the probability of a type II error is given by [3,4]

$$\beta_n = \exp\{-[nD(\rho_0||\rho_1) + \sqrt{nb}\Phi^{-1}(\delta) + O(\ln n)]\}, \quad (1)$$

where the term linear in n is given by the Umegaki quantum relative entropy [5]:

$$D(\rho_0||\rho_1) = \text{Tr}[\rho_0(\ln \rho_0 - \ln \rho_1)]. \quad (2)$$

Here we focus on the asymptotic regime of $n \gg 1$, where the dominant term is the relative entropy.

Returning to the problem of exoplanet detection, different experimental methodologies have been developed [6–8], including Doppler measurements, transit observation, gravitational microlensing, as well as direct

imaging. The different techniques are complementary: for example, Doppler and transit techniques preferentially detect planets that orbit closer to their stars and are larger in mass or size while microlensing and direct imaging (traditionally) are more sensitive to planets in further orbits [7,8].

Direct imaging (DI), being the most conceptually straightforward, is a powerful complementary technique to the others, especially when the planet is relatively far from the star [7,8]: a telescope is used to create a focused image of the star system, and the intensity profile is analyzed to determine whether a planet is present (Fig. 1). However, because of diffraction, the image of a pointlike object is not a point but will have a finite spread. Because of this blurring as well as the emission of exoplanets being weak compared to the bright object, detecting this emission in the proximity of the much

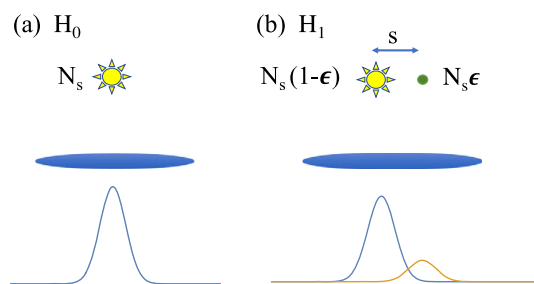


FIG. 1. An optical imaging system (modeled as a thin lens) is used to discern between two hypotheses. Hypothesis H_0 is that only one source is present of intensity N . Hypothesis H_1 is that two sources are present, with total intensity N and relative intensity $\epsilon/(1-\epsilon) \ll 1$. The field focused on the image screen can be measured by DI, or by applying an interferometric measurement, for example, SPADE [9] or SLIVER [10,11].

brighter stellar source presents the most severe practical obstacle to direct detection [7,8].

In this Letter, we use techniques from quantum imaging to boost the efficiency of exoplanet detection as a complement to DI. First, we use a fully quantum formalism to determine the ultimate limit of quantum imaging, as expressed by the quantum relative entropy. Then, we show that this ultimate limit can be achieved by a relatively simple, linear optical measurement, consisting of SPAtial DE-multiplexing (SPADE) or Super-Localization via Image-inVERsion interferometry (SLIVER). These measurements are already known to be optimal for other problems in quantum imaging [9–14].

We assume that N photons per detection window are collected and measured [Of course, one can also consider a model in which H_1 has a total mean photon number $N(1 + \epsilon)$, and photon number information is indeed used for the transit method [6]. Here we choose to preserve the total photon number because the mean photon number of the sources may not be known exactly.] These photons are either emitted by a star (H_0) or by a star-planet system (H_1). In the latter case a small fraction $\epsilon \ll 1$ of the light is scattered from the planet at an angle $s \ll 1$. Within this model, we show that the error exponent for quantum imaging is proportional to ϵ , whereas in DI it scales as ϵ^2 . This suggests a quadratic improvement of quantum over classical imaging.

Diffraction-limited direct imaging.—In conventional imaging, a converging optical system is used to create a focused image of an object. In the far-field and paraxial regime, the imaging system is characterized by the (normalized) point-spread function (PSF) $\psi(x - x_0)$, centered at x_0 , where x is the angular coordinate on the screen. For simplicity, we assume a one-dimensional scalar field and unit angular magnification [15]. We quantify the spread of the PSF using the parameter $\sigma := (1/2)[- \int \psi(x)\psi''(x)dx]^{-1/2}$. As discussed in Ref. [16], σ measures the uncertainty in localizing the emitter. For example, for the PSF $\psi(x) = (a\pi)^{-1/2} \sin(ax)/x$, $\sigma = \sqrt{3}/(2a)$, and for a Gaussian PSF, $\psi(x) = (2\pi\sigma^2)^{-1/4} \exp(-x^2/4\sigma^2)$, σ corresponds to the standard deviation.

Consider the null hypothesis where there is no planet orbiting the star. The intensity profile on the image screen is given by the square of the PSF, $p_0(x) = |\psi(x - x_0)|^2$, centered about the position, x_0 , of the star. On the other hand, if a planet is present, the intensity profile is

$$p_1(x) = (1 - \epsilon)|\psi(x - x_0)|^2 + \epsilon|\psi(x - x_0 - s)|^2, \quad (3)$$

where $\epsilon \ll 1$ is the relative intensity of the light scattered by the exoplanet, and s is its angular separation from the star. We assume that the two sources are incoherent.

In the limit of weak signals, $p_0(x)$ and $p_1(x)$ are the probabilities of detecting a photon at position x on the image screen. Exoplanet detection with DI is hence

equivalent to the problem of discriminating between the probability distributions p_0 and p_1 . On detecting n photons, by requiring that the probability of a false positive $\alpha_n \in (0, \delta)$ with $\delta < 1$, the probability β_n of a false negative decreases exponentially with n , where the asymptotic exponent is given by the classical version of Eq. (2) [17], where

$$D(p_0||p_1) = \int dx p_0(x) [\ln p_0(x) - \ln p_1(x)] \quad (4)$$

is the classical relative entropy.

The above error exponent can be computed given a specific form of the PSF. To make this more concrete, we assume a Gaussian PSF, which yields

$$D(p_0||p_1) = - \int dx |\psi(x)|^2 \ln \left(1 - \epsilon + \epsilon e^{\frac{2xs-s^2}{2\sigma^2}} \right). \quad (5)$$

In the limit that $\epsilon \ll 1$, and for $s \lesssim \sigma$,

$$D(p_0||p_1) \approx (e^{\frac{s^2}{2\sigma^2}} - 1) \frac{\epsilon^2}{2} + O(\epsilon^3). \quad (6)$$

The largest term in Eq. (6) is quadratic in both ϵ and s/σ . This formally expresses the challenges of using DI for exoplanet detection in a scenario in which the planet is much dimmer and is very close to the star.

Quantum-limited exoplanet detection.—It is known that quantum imaging beats DI for the problem of estimating the transverse separation between two faint sources [9]. Here we show that quantum-limited imaging also yields a quadratic improvement in the exponent of the type II error. We will first consider a model in which at most one photon arrives at a time; then in the ‘‘Thermal light’’ section, we describe the star-planet system as sources of thermal light. We denote as $a(x)$, $a(x)^\dagger$ the continuous set of annihilation and creation operators associated to a photon detected at the angle x on the image plane. Therefore, the state of a photon emitted by the star is $|\psi_{x_0}\rangle = \int dx \psi(x - x_0) a(x)^\dagger |0\rangle$, where $|0\rangle$ is the vacuum state. Similarly, the state of photon scattered by the planet is $|\psi_{x_0+s}\rangle = \int dx \psi(x - x_0 - s) a(x)^\dagger |0\rangle$, and the two hypotheses are associated with the density matrices

$$\rho_0 = |\psi_{x_0}\rangle \langle \psi_{x_0}|, \quad (7)$$

$$\rho_1 = (1 - \epsilon) |\psi_{x_0}\rangle \langle \psi_{x_0}| + \epsilon |\psi_{x_0+s}\rangle \langle \psi_{x_0+s}|. \quad (8)$$

From the above, we obtain the quantum relative entropy,

$$D(\rho_0\|\rho_1) = -\frac{[1-u-2\epsilon(1-\omega^2)]^2}{(1-u-2\epsilon)^2+4\epsilon(1-u-\epsilon)\omega^2}\ln\left(\frac{1-u}{2}\right) - \frac{[1+u-2\epsilon(1-\omega^2)]^2}{(1+u-2\epsilon)^2+4\epsilon(1+u-\epsilon)\omega^2}\ln\left(\frac{1+u}{2}\right), \quad (9)$$

where we have defined $\omega = \langle \psi_{x_0} | \psi_{x_0+s} \rangle$, and $u = \sqrt{1-4\epsilon(1-\epsilon)(1-\omega^2)}$. By expanding this expression around $\epsilon = 0$ we obtain

$$D(\rho_0\|\rho_1) = (1-\omega^2)\epsilon + O(\epsilon^2), \quad (10)$$

i.e., a quadratic improvement over DI. For a Gaussian PSF, $\omega^2 = \exp(-s^2/4\sigma^2)$.

Figure 2 plots Eqs. (5) and (9) vs ϵ (top) and s/σ (bottom). Both quantities approach the same limit when $s/\sigma \gg 1$, implying that DI is optimal for wide separations. Although both quantities become zero as $s \rightarrow 0$, they do with a different scaling. This means that DI becomes increasingly erroneous for close separations, whereas the optimal quantum strategy remains useful over a wider parameter range.

Optimality of interferometric measurements.—Here we show that interferometric measurements are optimal in the weak signal limit. Consider a SPADE measurement in which the field is split into its components along the Hermite-Gauss spatial modes, $\phi_q(x)$ [18], followed by modewise photodetection. This measurement may be

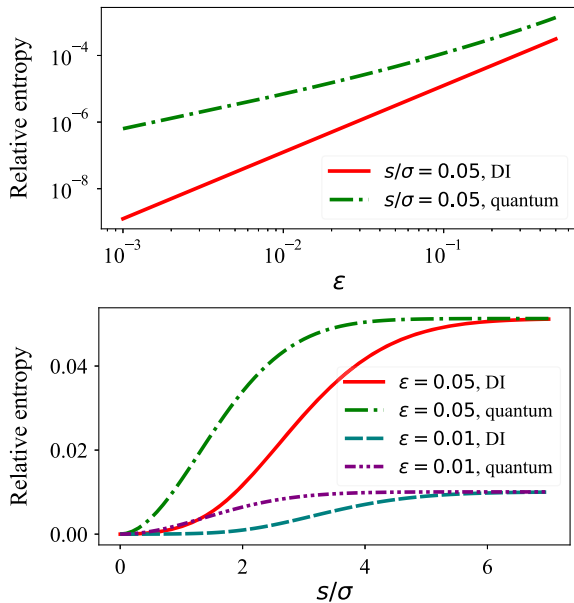


FIG. 2. Comparison between the quantum relative entropy and the relative entropy for DI. Top: the two quantities plotted vs ϵ , for $s/\sigma = 0.05$. The log-log scale emphasizes the different scaling for small ϵ . Bottom: the quantum and classical entropy plotted vs s/σ for different values of ϵ .

realized with an interferometric setup [12], a hologram [16], or a multimode waveguide [9]. This latter approach is shown schematically in Fig. 3. A state of a single photon in the q th mode reads $|\phi_q\rangle = \int \phi_q(x)a(x)^\dagger|0\rangle$. For a Gaussian PSF, centered in $x = x_0$, their overlap is

$$|\langle \phi_q | \psi_{x_0} \rangle|^2 = e^{-Q} \frac{Q^q}{q!}, \quad Q = \frac{x_0^2}{4\sigma^2}. \quad (11)$$

For our case, we point the optical imaging system toward the optical center of mass,

$$\bar{x} = (1-\epsilon)x_0 + \epsilon(x_0 + s). \quad (12)$$

With respect to \bar{x} , the relative position of the star is $(-\epsilon s)$, and the planet is positioned at $(1-\epsilon)s$. Therefore,

$$|\langle \phi_q | \psi_{\text{star}} \rangle|^2 = \frac{1}{q!} e^{-\frac{\epsilon^2 s^2}{4\sigma^2}} \left(\frac{\epsilon s}{2\sigma}\right)^{2q}, \quad (13)$$

$$|\langle \phi_q | \psi_{\text{planet}} \rangle|^2 = \frac{1}{q!} e^{-\frac{(1-\epsilon)^2 s^2}{4\sigma^2}} \left(\frac{(1-\epsilon)s}{2\sigma}\right)^{2q}. \quad (14)$$

From this, we obtain the probability of detecting the photon in the q th Hermite-Gauss spatial mode:

$$p_1(q) = (1-\epsilon)|\langle \phi_q | \psi_{\text{star}} \rangle|^2 + \epsilon|\langle \phi_q | \psi_{\text{planet}} \rangle|^2. \quad (15)$$

If the planet is absent (H_0), the center of mass coincides with the position of the star, i.e., $\bar{x} = x_0$, and the probability is $p_0(q=0) = |\langle \phi_0 | \psi_{\text{star}} \rangle|^2 = 1$. The exponent for type II error is thus obtained from the relative entropy between these two probability distributions. We have

$$D(p_0\|p_1) = -\ln p_1(0) \approx \left(1 - e^{-\frac{s^2}{4\sigma^2}}\right)\epsilon + O(\epsilon^2), \quad (16)$$

which is optimal in the limit of small ϵ , as it coincides with the quantum relative entropy. This result follows directly from the fact that the Gaussian PSF equals the fundamental ($q=0$) Hermit-Gaussian function. To achieve an optimal alignment, one can use an iterative technique: once the centroid of the system is determined with a camera, it is

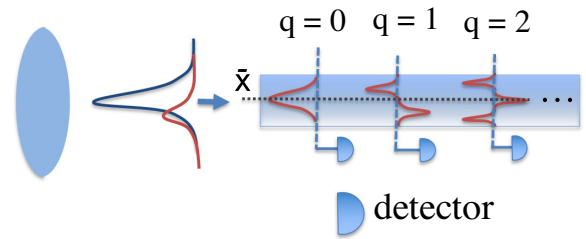


FIG. 3. A multimode waveguide can be used as Hermite-Gauss mode sorter [9]. The optical center of mass of the two sources, \bar{x} , is aligned with the center of the waveguide.

aligned with the SPADE device; the position can be adjusted until the received state maximally couples into the fundamental mode.

In general, the PSF is not Gaussian and it may not coincide with the fundamental mode of the basis used for SPADE. In this more general case, an optimal interferometric measurement is obtained from a parity measurement, i.e., by inversion imaging, also known as SLIVER, as long as the PSF is even, $\psi(x) = \psi(-x)$. It follows that, if H_0 is true, the probability of measuring even parity is $\pi_0(0) = 1$, and the probability of odd parity is $\pi_0(1) = 0$.

To see what happens when H_1 is true, first consider a single emitter displaced by δx . We can write the displaced PSF $\psi(x - \delta x)$ as a sum of even and odd functions,

$$\begin{aligned} \psi(x - \delta x) &= \frac{1}{2} [\psi(x - \delta x) + \psi(x + \delta x)] \\ &\quad + \frac{1}{2} [\psi(x - \delta x) - \psi(x + \delta x)]. \end{aligned} \quad (17)$$

A parity measurement then yields an even outcome with probability $\pi(0) = \frac{1}{4} \int |\psi(x - \delta x) + \psi(x + \delta x)|^2 dx$. By expanding around $\delta x = 0$ we obtain

$$\pi(0) = 1 + \delta x^2 \int \psi(x) \psi''(x) dx + O(\delta x^3). \quad (18)$$

Coming back to hypothesis H_1 , as the two emitters are incoherent, the probability of measuring an even parity is, for small ϵ and s ,

$$\pi_1(0) \simeq (1 - \epsilon) \left(1 - \frac{\epsilon^2 s^2}{4\sigma^2} \right) + \epsilon \left(1 - \frac{(1 - \epsilon)^2 s^2}{4\sigma^2} \right), \quad (19)$$

where we have used the fact that σ is defined such that $\int \psi(x) \psi''(x) dx = 1/4\sigma^2$. Finally, the relative entropy for this parity measurement is $D(\pi_0 \| \pi_1) = -\ln \pi_1(0) = s^2 \epsilon / 4\sigma^2 + O(\epsilon^2)$, which is optimal for small ϵ and s .

Thermal light.—In reality, the states received are thermal [19], and the probabilities of getting more than one photon on the image screen are nonzero. We can describe such a state of light using the Gaussian state formalism [20], and the problem becomes that of Gaussian hypothesis testing [21].

Consider n bosonic modes with quadrature operators $\hat{X} = (\hat{q}_1, \dots, \hat{q}_n, \hat{p}_1, \dots, \hat{p}_n)$, which satisfy canonical commutation relations. The entries of the covariance matrix (CM) of a state are given by $V_{jk} = \frac{1}{2} \text{Tr}[\rho \{ \hat{X}_j - \langle \hat{X}_j \rangle, \hat{X}_k - \langle \hat{X}_k \rangle \}]$. The Williamson decomposition of the CM reads $V = U((\bigoplus_{j=1}^n \nu_j) \otimes \mathbb{1}_2) U^T$, where $\nu_j = \bar{n}_j + 1/2$, \bar{n}_j is the mean photon number of the mode j , and U is a symplectic matrix [20]. The quantum relative entropy of two Gaussian states with zero displacement is given by [22]

$$D(\rho_0 \| \rho_1) = -S(\rho_0) + \Sigma(V_0, V_1), \quad (20)$$

where $2\Sigma(V_0, V_1) = \ln[\det(V_1 + i\Omega/2)] + \text{Tr}[V_0 G_1]$, and $G_1 = 2i\Omega \coth^{-1}(2V_1 i\Omega)$. Here S is the von Neumann entropy, $S(\rho) = -\sum_{j=1}^n h(\bar{n}_j)$, with $h(y) = (y+1)\ln(y+1) - y\ln(y)$ [20].

The two quasimonochromatic point sources are associated with the creation and annihilation operators \hat{q}_1, \hat{p}_1 and \hat{q}_2, \hat{p}_2 . The imaging system maps the source operators onto the image-screen operators \hat{q}'_1, \hat{p}'_1 and \hat{q}'_2, \hat{p}'_2 . In fact, the image modes are attenuated by a factor η [11], $\hat{q}'_j \rightarrow \sqrt{\eta} \hat{q}_j + \sqrt{1-\eta} \hat{q}_{e_j}$ (for $j = 1, 2$, plus similar relations for the operators \hat{p}'_1, \hat{p}'_2), where \hat{q}_{e_j} are vacuum mode operators accounting for loss; η is the loss parameter due to free-space propagation. The image-plane modes do not commute due to diffraction; in fact we have $[\hat{q}'_1, \hat{q}'_2] = \int \psi(x) \psi(x+s) dx = \omega$. We can define commuting image-plane quadrature operators by taking their sum and differences

$$\hat{q}'_{\pm} = \frac{\hat{q}'_1 \pm \hat{q}'_2}{\sqrt{2(1 \pm \omega)}}, \quad \hat{p}'_{\pm} = \frac{\hat{p}'_1 \pm \hat{p}'_2}{\sqrt{2(1 \pm \omega)}}. \quad (21)$$

The CM of these quadratures reads (see Supplemental Material [23])

$$V = \begin{pmatrix} \mu_+ & \nu & 0 & 0 \\ \nu & \mu_+ & 0 & 0 \\ 0 & 0 & \mu_- & \nu \\ 0 & 0 & \nu & \mu_- \end{pmatrix}, \quad (22)$$

where $\mu_{\pm} = \frac{1}{2}((1 \pm \omega)N + 1)$ and $\nu = (N/2)\sqrt{1 - \omega^2}(1 - 2\epsilon)$.

We can now substitute Eq. (22) into (20) to compute the quantum relative entropy, where the hypothesis H_0 is obtained by putting $\epsilon = 0$.

We leave the full expression for $D(\rho_0 \| \rho_1)$ in the Supplemental Material [36]. In the limit $\epsilon \ll 1$, we obtain

$$D(\rho_0 \| \rho_1) \approx N(1 - \omega^2)\epsilon, \quad (23)$$

which is linear in both ϵ and N . This result allows us to draw a number of conclusions. First, the quantum relative entropy scales linearly with ϵ even for generic values of the mean number of thermal photons, and not only for small N . Second, as expected, the quantum relative entropy per photon, $D(\rho_0 \| \rho_1)/N$, approaches that of the single photon, given by Eq. (2). We observe numerically that $D(\rho_0 \| \rho_1)/N$ is qualitatively very similar to the single-photon relative entropy shown in Fig. 2. Furthermore, it only mildly depends on N , as it does not drop significantly by increasing N . The performance of SPADE for thermal sources is scaled by a factor of $1/(1+N)$ (see Supplemental Material [23]), which remains optimal in

the limit $N \ll 1$, as typical for astronomical observations [19].

Conclusions.—We have discussed asymmetric hypothesis testing in the context of shot-noise-limited imaging. The hypothesis under scrutiny was the existence of an exoplanet orbiting a star, and we aimed to minimize the probability of a false negative. Compared to direct imaging, we have shown that interferometric measurements yield a quadratic improvement in the error exponent. As an example, the exoplanet LkCa 15 c [24] has angular separation $s \approx 0.068$ arcsec [25], and it was observed with an instrument with variable baselines ranging from 1.4 to 7.0 m, at wavelengths $2.18 \mu\text{m}$ and $3.8 \mu\text{m}$. When operating in imaging mode, assuming that the PSF is a two-dimensional Airy function, this yields s/σ in the range from 0.34 to 2.97. This suggests that our approach could be used to improve the detection efficiency of DI, or to extend the range of applications of DI toward smaller angular separations.

Beyond exoplanet detection, our theory applies to the detection of the presence of a secondary emitter in other settings. An example is dimer detection in microscopy [26]. Our results also complement previous works on super-resolution imaging, whose goal was to estimate a sub-wavelength separation between two sources (see, e.g., Refs. [9,11,27,28]). In fact, before measuring the separation, one needs to ensure that there are two sources and not just one. Our work discusses how this can be done optimally. Furthermore, we remark that interferometric measurements such as SPADE and SLIVER are optimal for both detecting the presence of the secondary sources and for estimating the separation.

Our work paves the way to a number of research questions, some of which may be addressed by reformulating our theory in the language of Poisson quantum information [29]. What is the effect of noise, e.g., dark counts [30–32] and cross-talk [33]? What is the relation with symmetric hypothesis testing, previously considered in the imaging optical setup in Ref. [34] (see also [35])? Furthermore, the optimality of SPADE and SLIVER suggests that other interferometric measurements may as well yield an optimal scaling of the error exponent [27]. Finally, we have considered the asymptotic limit of many detection events, yet we expect that similar results hold for a finite data sample, a regime that can be explored using Renyi entropies [36].

Z. H. is supported by a Sydney Quantum Academy Postdoctoral Fellowship. C. L. is supported by the EPSRC Quantum Communications Hub, Grant No. EP/T001011/1. This work is funded in part by the EPSRC grant Large Baseline Quantum-Enhanced Imaging Networks, Grant No. EP/V021303/1. We thank Pieter Kok, Christian Schwab, Stefano Pirandola, and Martin Plenio for insightful feedback.

- [1] F. Hiai and D. Petz, *Commun. Math. Phys.* **143**, 99 (1991).
- [2] O. T. and H. Nagaoka, *IEEE Trans. Inf. Theory* **46**, 2428 (2000).
- [3] K. Li *et al.*, *Ann. Stat.* **42**, 171 (2014).
- [4] M. Tomamichel and M. Hayashi, *IEEE Trans. Inf. Theory* **59**, 7693 (2013).
- [5] M. M. Wilde, *Quantum Information Theory* (Cambridge University Press, Cambridge, England, 2013).
- [6] M. Perryman, *The Exoplanet Handbook* (Cambridge University Press, Cambridge, England, 2018).
- [7] J. T. Wright and B. S. Gaudi, *Exoplanet Detection Methods* (2013), p. 489, <https://arxiv.org/abs/1210.2471>.
- [8] D. A. Fischer, A. W. Howard, G. P. Laughlin, B. Macintosh, S. Mahadevan, J. Sahlmann, and J. C. Yee, *Protostars & Planets VI*, edited by H. Beuther, R. S. Klessen, C. P. Dullemond, and T. Henning (University of Arizona Press, Tucson, 2014), Vol. 914, pp. 715–737, <https://arxiv.org/abs/1505.06869>.
- [9] M. Tsang, R. Nair, and X.-M. Lu, *Phys. Rev. X* **6**, 031033 (2016).
- [10] R. Nair and M. Tsang, *Phys. Rev. Lett.* **117**, 190801 (2016).
- [11] C. Lupo and S. Pirandola, *Phys. Rev. Lett.* **117**, 190802 (2016).
- [12] M. Tsang, *Contemp. Phys.* **60**, 279 (2019).
- [13] F. Tamburini, G. Anzolin, G. Umbrico, A. Bianchini, and C. Barbieri, *Phys. Rev. Lett.* **97**, 163903 (2006).
- [14] K. Wicker and R. Heintzmann, *Opt. Express* **15**, 12206 (2007).
- [15] J. Goodman, *Introduction to Fourier optics* (McGraw-Hill, New York, 2008).
- [16] M. Pařr, B. Stoklasa, Z. Hradil, L. L. Sánchez-Soto, and J. Rehacek, *Optica* **3**, 1144 (2016).
- [17] T. M. Cover and J. A. Thomas, *Elements of Information Theory*, 2nd ed., Wiley Series in Telecommunications and Signal Processing (Wiley-Blackwell, New York, 2006).
- [18] A. Yariv, *Quantum Electronics* (Wiley, New York, 1989).
- [19] L. Mandel and E. Wolf, *Optical Coherence and Quantum Optics* (Cambridge University Press, Cambridge, England, 1995).
- [20] A. Serafini, *Quantum Continuous Variables: A Primer of Theoretical Methods* (CRC Press, Boca Raton, FL, 2017).
- [21] M. M. Wilde, M. Tomamichel, S. Lloyd, and M. Berta, *Phys. Rev. Lett.* **119**, 120501 (2017).
- [22] S. Pirandola, R. Laurenza, C. Ottaviani, and L. Banchi, *Nat. Commun.* **8**, 15043 (2017).
- [23] See Supplemental Material at <http://link.aps.org/supplemental/10.1103/PhysRevLett.127.130502> for details of the calculation.
- [24] S. Sallum, K. Follette, J. A. Eisner, L. M. Close, P. Hinz, K. Kratter, J. Males, A. Skemer, B. Macintosh, P. Tuthill *et al.*, *Nature (London)* **527**, 342 (2015).
- [25] Nasa exoplanet archive, direct imaging.
- [26] X. Nan, E. A. Collisson, S. Lewis, J. Huang, T. M. Tamgüney, J. T. Liphardt, F. McCormick, J. W. Gray, and S. Chu, *Proc. Natl. Acad. Sci. U.S.A.* **110**, 18519 (2013).
- [27] C. Lupo, Z. Huang, and P. Kok, *Phys. Rev. Lett.* **124**, 080503 (2020).

- [28] W.-K. Tham, H. Ferretti, and A. M. Steinberg, *Phys. Rev. Lett.* **118**, 070801 (2017).
- [29] M. Tsang, [arXiv:2103.08532](https://arxiv.org/abs/2103.08532).
- [30] Y. L. Len, C. Datta, M. Parniak, and K. Banaszek, *Int. J. Quantum. Inform.* **18**, 1941015 (2020).
- [31] C. Lupo, *Phys. Rev. A* **101**, 022323 (2020).
- [32] C. Oh, S. Zhou, Y. Wong, and L. Jiang, *Phys. Rev. Lett.* **126**, 120502 (2021).
- [33] M. Gessner, C. Fabre, and N. Treps, *Phys. Rev. Lett.* **125**, 100501 (2020).
- [34] X.-M. Lu, H. Krovi, R. Nair, S. Guha, and J. H. Shapiro, *npj Quantum Inf.* **4**, 64 (2018).
- [35] M. R. Grace and S. Guha, [arXiv:2107.00673](https://arxiv.org/abs/2107.00673).
- [36] K. P. Seshadreesan, L. Lami, and M. M. Wilde, *J. Math. Phys. (N.Y.)* **59**, 072204 (2018).